

Document downloaded from:

<http://hdl.handle.net/10251/183625>

This paper must be cited as:

Khan, F.; Barrera, D.; Sales Maicas, S.; Misra, S. (2021). Curvature, twist and pose measurements using fiber Bragg gratings in multi-core fiber: A comparative study between helical and straight core fibers. *Sensors and Actuators A Physical*. 317:1-7.  
<https://doi.org/10.1016/j.sna.2020.112442>



The final publication is available at

<https://doi.org/10.1016/j.sna.2020.112442>

Copyright Elsevier

Additional Information

# Curvature, Twist and Pose Measurements using Fiber Bragg Gratings in Multi-Core Fiber: A Comparative Study between Helical and Straight Core Fibers

Fouzia Khan<sup>a,\*</sup>, David Barrera<sup>b</sup>, Salvador Sales<sup>c</sup>, Sarthak Misra<sup>a</sup>

<sup>a</sup>*Surgical Robotics Laboratory, Department of Biomedical Engineering, University of Groningen and University of Medical Center Groningen, 9713 GZ, The Netherlands.  
Department of Biomechanical Engineering, Engineering Technology, University of Twente,  
7522 NB, The Netherlands.*

<sup>b</sup>*Department of Electronics, University of Alcalá, Alcalá de Henares, 28805, Spain.*

<sup>c</sup>*ITEAM Research Institute, Universitat Politècnica de València, Camino de Vera, 46022  
València, Spain.*

---

## Abstract

This paper presents a technique to acquire measurements of curvature, twist and pose for two multi-core fibers; one with straight cores and the other with helical cores. Both the fibers have multiple fiber Bragg grating (FBG) sensors inscribed in the cores and the fibers are placed in known configurations in order to compare their measurement accuracy. For the curvature measurements both the fibers are placed in constant curvature slots; for the twist measurements, a set of twists are applied to each fiber and for the pose measurements the fibers are placed in moulds of different shape. The mean curvature errors are  $0.22 \text{ m}^{-1}$  and  $0.13 \text{ m}^{-1}$ , in the helical and straight core fiber respectively. For the twist measurement the mean errors are 26.57 degrees/m and 146.50 degrees/m in the helical and straight core fiber, respectively. Lastly, the pose measurement consists of position and orientation where the orientation is represented in the axis-angle form. The mean position errors are 0.49 mm and 0.27 mm, the mean

---

\*This project has received funding from the European Union's Horizon 2020 research and innovation programme under grant agreement #688279 (EDEN2020). It was also partially supported by the Spanish Ministry of Economy and Competitiveness under the project DIMENSION TEC2017-88029- R. The work of D. Barrera was supported by Spanish MICINN fellowship IJCI-2017-32476. The funding sources were not involved in the research nor in the preparation of the article.

\*Corresponding author

*Email address:* `f.khan@utwente.nl` (Fouzia Khan)

axis orientation errors are 0.12 degrees and 0.26 degrees and the mean angle orientation errors are 1.10 degrees and 1.18 degrees, for the helical and straight core fiber, respectively. The results show that the twist measurement error is significantly low with the helical core fiber, thus helical core fiber is better suited than straight core fiber for applications where twist measurements are required.

*Keywords:* curvature, twist, pose, reconstruction, fiber Bragg grating, optical sensing, elastic rod model, helical core fiber, spun core fiber, twisted core fiber

---

## 1. Introduction

Fiber Bragg gratings (FBG) have been applied in various fields such as oil and gas industry, security, structural health monitoring and have promising applications for monitoring medical instruments [1] [2]. This is due to their compactness, light weight, flexibility, tensile strength, immunity to electromagnetic interference and high tolerance to temperature [3]. This study focuses on application of the FBG sensors for curvature, twist and pose measurements of minimally invasive medical instruments. Spatial information of minimally invasive instruments during medical procedures is essential for accurate navigation. The instrument's tip pose, which is the position and orientation, is particularly important for avoiding critical structures inside the body. Currently, this information is commonly acquired using fluoroscopy or ultrasound. However, the instruments can be difficult to observe in ultrasound due to artifacts and low resolution, while fluoroscopy exposes patients to harmful radiation. These issues are mitigated with the use of FBG sensors because they are safe and can provide good resolution data in space and time; thus these sensors are an attractive alternative [4].

In the literature, several studies have validated the use of FBG sensors inscribed in optical fibers for position measurements and its application in medical procedures [1, 5, 6, 7, 8]. Nevertheless, Duncan *et. al* have observed error in position measurement from FBG sensors in straight core fiber due to their insufficient sensitivity to twist [9]. In order to acquire more accurate twist

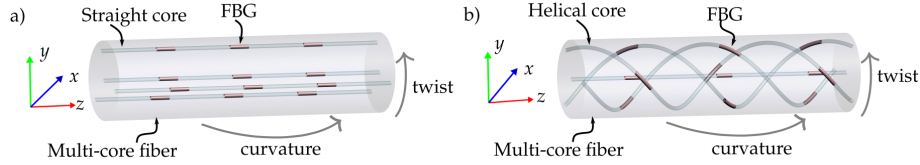


Figure 1: a) Straight core fiber with three sets of co-located fiber Bragg grating (FBG) sensors. b) Helical core fiber with three sets of co-located FBG sensors. Curvature is induced due to a torque about a vector in the x-y plane and twist is due to torque about the z-axis.

measurement researchers have inscribed FBG sensors on helical core fibers and validated its accuracy as twist sensors [3, 4, 10, 7, 11, 12]. However, a comparison in measurement accuracy between FBG sensors in helical core fiber and in straight core fiber has not been presented [13]. In this study, the measurement accuracy of curvature, twist and pose are presented for both helical and straight core fiber. Each fiber has multiple sets of co-located FBG sensors as shown in Figure 1. The results show that the helical core fiber is better suited than the straight core fiber for applications with twist. The main contributions of this study are the application of an elastic rod model to the helical core fiber in order to acquire the pose of the tip and the comparative study of the measurement accuracy between the helical and straight core fiber. The theoretical background utilized to acquire the results, and description of the experiments are presented in Sections 2 and 3, respectively.

## 2. Theoretical Background

The technique to acquire the curvature, twist and pose measurements using FBG sensors in the multi-core fibers with helical and straight cores is presented in this section. It is based on mechanics of materials and the elastic rod theory [14, 15]. The curvature and twist is determined from the strain on the fiber. According to the mechanics of materials, the fiber's curvature is related to its

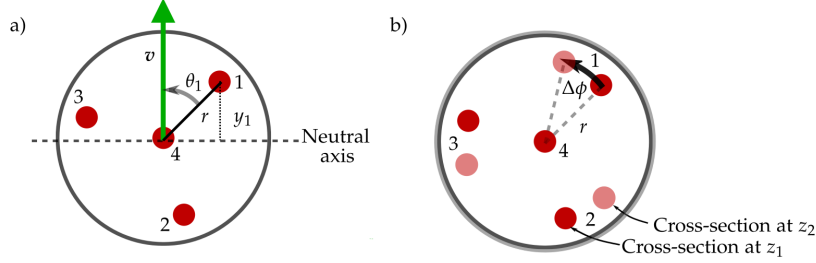


Figure 2: Cross-section of the straight core fiber and the helical core fiber with numerical labels  $\{1, 2, 3, 4\}$  for the cores. a) Parameters for curvature measurement.  $\mathbf{v} \in \mathbb{R}^2$  is the curvature vector,  $\|\mathbf{v}\| = \kappa \in \mathbb{R}$ ,  $\theta_1 \in \mathbb{R}$  is the angle between core 1 and the curvature vector,  $r \in \mathbb{R}$  is the radial distance to the cores,  $y_1 \in \mathbb{R}$  is the perpendicular distance from core 1 to the neutral axis. b) Parameters for twist measurement. Overlay of two cross sections of the fiber, one at arc length  $z_1 \in \mathbb{R}_{>0}$  and the other at  $z_2 \in \mathbb{R}_{>0}$ ,  $\Delta z = z_2 - z_1$ . An applied twist will cause the cross sections to be rotated with respect to each other, this rotation is  $\Delta\phi \in \mathbb{R}$ .

normal strain and its twist to its shear strain by the following equations [15]:

$$\epsilon_\kappa = -\kappa y, \quad (1)$$

$$\epsilon_\tau = G \frac{\Delta\phi}{\Delta z} r, \quad (2)$$

where,  $\epsilon_\kappa \in \mathbb{R}$  is the strain due to curvature,  $\kappa \in \mathbb{R}_{\geq 0}$  is the curvature value,  $y \in \mathbb{R}_{\geq 0}$  is the perpendicular distance between the neutral axis and the location of the strain on the cross section. The strain due to the twist is  $\epsilon_\tau \in \mathbb{R}$  at a radial  
40 distance  $r \in \mathbb{R}_{>0}$  and  $G \in \mathbb{R}_{>0}$  is the material constant relating shear strain with angular difference. The applied twist will cause the cross sections along the arc length of the fiber to rotate with respect to each other. The angular change between two cross sections is given by  $\Delta\phi \in \mathbb{R}$  and the difference in arc length between those cross sections is  $\Delta z \in \mathbb{R}_{>0}$ .  $\Delta z = z_2 - z_1$  in Figure 2,  
45 which illustrates the variables in (1)-(2) on the multi-core fiber cross-section.

The strains on the fiber can be calculated from the measured Bragg wavelength of the FBG sensors. In this study, the sensors are placed along the fiber such that there are sets of four co-located sensors, which means there are four sensors at particular cross sections of the fiber. These sensors enable measure-

50 ments of strains at four locations on the cross section, as shown in Figure 2. These strain measurements can be used to solve for the curvature and twist. The relation between strain and the Bragg wavelength of an FBG sensor can be approximated with the following linear equation [16]:

$$\frac{\Delta\lambda_{B0}}{\lambda_{B0}} = S(\epsilon - \epsilon_0), \quad (3)$$

where,  $\lambda_{B0} \in \mathbb{R}$  and  $\epsilon_0 \in \mathbb{R}$  are the initial values of the Bragg wavelength and strain, respectively.  $S \in \mathbb{R}_{>0}$  is the gauge factor and  $\epsilon \in \mathbb{R}$  is the strain. However, a general relation that also incorporates the temperature is the following [17]:

$$\ln \frac{\lambda_B}{\lambda_{B0}} = S(\epsilon - \epsilon_0) + \Sigma(T - T_0), \quad (4)$$

where,  $\lambda_B \in \mathbb{R}$  is the measured Bragg wavelength,  $\Sigma \in \mathbb{R}_{>0}$  is the temperature sensitivity,  $T \in \mathbb{R}$  is temperature, and  $T_0 \in \mathbb{R}$  is the initial temperature. 55

The strain on the external cores, shown as cores 1-3 in Figure 2, is due to both curvature and twist; whereas the strain on the central core, labeled 4, is theoretically zero since it is at the center of the cross section. Any change in Bragg wavelength of sensor 4 is due to change in temperature, thus it can be used to eliminate the effect of temperature in cores 1-3. The strain due to twist is the same on the sensors 1-3 and since they are  $\frac{2\pi}{3}$  radians apart the mean of the three sensors will give the strain due to twist, see Appendix A for details. The remainder of the strain on cores 1-3 is due to the curvature. Thus, the following equations hold:

$$\epsilon_{i\kappa} = -\kappa r \cos\left(\theta_1 + \frac{2\pi}{3}(i-1)\right) \quad (5)$$

$$\epsilon_\tau = \frac{1}{3S} \sum_{i=1}^3 m_{i\Delta\epsilon} \quad (6)$$

where  $i \in \{1, 2, 3\}$  is the sensor number,  $\epsilon_{i\kappa} \in \mathbb{R}$  is the strain due to curvature  $\kappa$  on the FBG sensor in core  $i$ ,  $r$  is the radial distance to the cores,  $\theta_1 \in \mathbb{R}$  is the angle between the vector from center to core 1 and the curvature vector  $\mathbf{v}$ ,  $\epsilon_\tau \in \mathbb{R}$  is the strain on the cores due to twist,  $S$  is the gauge factor of the FBG

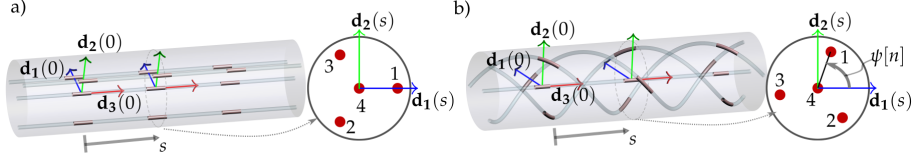


Figure 3: Schematic of the straight core fiber and the helical core fiber with the material frames  $\{\mathbf{d}_1(s) \in \mathbb{R}^3, \mathbf{d}_2(s) \in \mathbb{R}^3, \mathbf{d}_3(s) \in \mathbb{R}^3\}$  are shown in a) and b), respectively. The arc length of the fiber is parameterized by  $s \in \mathbb{R}$ , the sensor set number is parameterized by  $n \in \mathbb{Z}$ ,  $\psi[n] \in \mathbb{R}$  is the angle between  $\mathbf{d}_1$  and core 1 in set  $n$ .

sensors,  $m_i \Delta \epsilon = m_i - m_4$  and  $m_i \in \mathbb{R}$  is  $\ln \frac{\lambda_B}{\lambda_{B0}}$ , which is the measurement from sensor  $i$ . The curvature  $\kappa$  and twist  $\Delta \phi$  can be evaluated as:

$$\kappa = \sqrt{v_1^2 + v_2^2} \quad (7)$$

$$\Delta \phi = \epsilon_\tau \frac{\Delta z}{Gr} \quad (8)$$

$$\text{where, } \mathbf{v} = \begin{bmatrix} v_1 \\ v_2 \end{bmatrix} = \begin{bmatrix} \kappa \cos(\theta_1) \\ \kappa \sin(\theta_1) \end{bmatrix} = \mathbf{C}^\dagger \boldsymbol{\zeta}, \quad \mathbf{C} = \begin{bmatrix} -Sr & 0 \\ \frac{1}{2}Sr & \frac{\sqrt{3}}{2}Sr \\ \frac{1}{2}Sr & -\frac{\sqrt{3}}{2}Sr \end{bmatrix}, \quad \boldsymbol{\zeta} = \begin{bmatrix} \zeta_1 \\ \zeta_2 \\ \zeta_3 \end{bmatrix}$$

$\mathbf{C}^\dagger$  is the Moore-Penrose pseudo-inverse of  $\mathbf{C}$  and  $\zeta_i = m_i - m_4 - S\epsilon_\tau$ . Appendix A contains the derivations of (5)-(8).

The fiber's pose can be reconstructed using the curvature vectors and the twist values that are evaluated along its length. Let  $n \in \mathbb{Z}_{>0}$  be the number of co-located sets of sensors. Then, the curvature vectors  $\mathbf{v}[n]$  and twist values  $\Delta \phi[n]$  can be acquired using (7) and (8). In this study  $\Delta \phi[1]$  is set to be zero. The fiber is modeled as an elastic rod with the center-line represented by a unit-speed curve  $\boldsymbol{\gamma}(s) \in \mathbb{R}^3$  and the material frames given by a set of orthonormal vectors  $\{\mathbf{d}_1(s) \in \mathbb{R}^3, \mathbf{d}_2(s) \in \mathbb{R}^3, \mathbf{d}_3(s) \in \mathbb{R}^3\}$ , where  $s \in \mathbb{R}_{\geq 0}$  is the parameter for the arc length of the fiber, as illustrated in Figure 3. The equations for an

elastic rod are as follows:

$$\frac{d}{ds}\boldsymbol{\gamma}(s) = \mathbf{d}_3(s) \quad (9)$$

$$\frac{d}{ds}\mathbf{d}_1(s) = \tilde{\phi}(s)\mathbf{d}_2(s) - \tilde{\chi}_2(s)\mathbf{d}_3(s) \quad (10)$$

$$\frac{d}{ds}\mathbf{d}_2(s) = -\tilde{\phi}(s)\mathbf{d}_1(s) + \tilde{\chi}_1(s)\mathbf{d}_3(s) \quad (11)$$

$$\frac{d}{ds}\mathbf{d}_3(s) = \tilde{\chi}_2(s)\mathbf{d}_1(s) - \tilde{\chi}_1(s)\mathbf{d}_2(s) \quad (12)$$

where,  $\tilde{\phi}(s) \in \mathbb{R}$ ,  $\tilde{\chi}_1(s) \in \mathbb{R}$  and  $\tilde{\chi}_2(s) \in \mathbb{R}$  are the rotations of the center-line  $\boldsymbol{\gamma}(s) \in \mathbb{R}^3$  about  $\mathbf{d}_3(s)$ ,  $\mathbf{d}_1(s)$  and  $\mathbf{d}_2(s)$ , respectively [14]. These rotations are related to the curvature  $\mathbf{v}[n]$  and twist  $\Delta\phi[n]$  calculated from the FBG sensors. For both the helical and straight core fiber, linearly interpolating  $\Delta\phi[n]$  over the arc length  $s$  gives the rotation about  $\mathbf{d}_3(s)$  which is  $\tilde{\phi}(s)$ . Similarly, for the straight core fiber, linear interpolation of  $v_1[n]$  and  $v_2[n]$  gives  $\tilde{\chi}_1(s)$  and  $\tilde{\chi}_2(s)$ , respectively. However, for the helical core fiber since  $\mathbf{d}_1(s)$  does not coincide with core 1 for all  $s$ , the calculated curvature vector  $\mathbf{v}[n]$  must be adjusted such that it is with respect to the material frame. This is achieved by subtracting the angle  $\psi[n] \in \mathbb{R}$  between  $\mathbf{d}_1$  and core 1 on cross-section of the sensor set  $n$  from  $\theta_1[n]$ , see Figure 3. The angle  $\psi[n]$  is related to the rate at which the fiber is twisted in order to create the helical cores. Thus,  $\psi[n]$  can be either calculated from the twist rate or deduced experimentally. For the helical core fiber  $\tilde{\chi}_1(s)$  and  $\tilde{\chi}_2(s)$  are interpolation of  $\chi_1[n] = \kappa[n]\cos(\theta_1[n] - \psi[n])$  and  $\chi_2[n] = \kappa[n]\sin(\theta_1[n] - \psi[n])$ , respectively. Then, the pose of both the fibers can be acquired using the discretized solution of (9)-(12) which is:

$$\mathbf{X}(s + \Delta s) = \mathbf{X}(s) \exp(\mathbf{A}(s)\Delta s), \quad (13)$$

$$\text{where, } \mathbf{X}(s) = \begin{bmatrix} \mathbf{d}_1(s) & \mathbf{d}_2(s) & \mathbf{d}_3(s) & \boldsymbol{\gamma}(s) \\ 0 & 0 & 0 & 1 \end{bmatrix},$$

$$\mathbf{A}(s) = \begin{bmatrix} 0 & -\tilde{\phi}(s) & \tilde{\chi}_2(s) & 0 \\ \tilde{\phi}(s) & 0 & -\tilde{\chi}_1(s) & 0 \\ -\tilde{\chi}_2(s) & \tilde{\chi}_1(s) & 0 & 1 \\ 0 & 0 & 0 & 0 \end{bmatrix},$$



$\boldsymbol{\gamma}(0) = [0\ 0\ 0]^T$ ,  $\mathbf{d}_1(0) = [1\ 0\ 0]^T$ ,  $\mathbf{d}_2(0) = [0\ 1\ 0]^T$ , and  $\mathbf{d}_3(0) = [0\ 0\ 1]^T$  [18].

The fiber tip position is  $\boldsymbol{\gamma}(L)$  and tip orientation in matrix form is  $[\mathbf{d}_1(L)\ \mathbf{d}_2(L)\ \mathbf{d}_3(L)]$ ,  
60 where  $L$  is the length of the fiber. The equations for acquiring the curvature, twist and pose measurements are validated through a set of experiments which are presented in the next section.

### 3. Experiments and Results

The equations presented in the previous section are utilized in three ex-  
65 periments that are conducted to compare the curvature, twist, and pose measurement accuracy between two multi-core fibers, one with helical cores and another with straight cores. [The FBG sensors in both the fibers are inscribed using phase masks and ultra-violet laser.](#) They are inscribed in the multi-core fiber with straight cores in-house and in the multi-core fiber with helical cores  
70 by Fujikura (Tokyo, Japan). Table 1 lists the specifications of the fibers. [The insertion loss of the straight core fiber including the fan-out is 1.5 dB and of the helical core fiber including the fan out is 2.2 dB.](#) There are 8 sets of FBG sensors, where each set consists of four co-located sensors that have the same Bragg wavelength. In the straight core fiber, the Bragg wavelengths range from 1537  
75 nm to 1554 nm with an increment of approximately 2 nm. In the helical core fiber, the Bragg wavelengths range from 1542 nm to 1556 nm with an increment of approximately 2 nm. The light source and the spectrum analyzer for the sensors are provided by the interrogator FBG-804D (FBGS International NV, Geel). The wavelength data is processed offline in Matlab 2017b (MathWorks,  
80 Massachusetts).

#### 3.1. Curvature

The experiments for curvature accuracy utilizes an acrylic board with seven fixed curvature slots that range from  $1.33\ \text{m}^{-1}$  to  $5.71\ \text{m}^{-1}$ . These slots are created using laser cutter and then smoothed by fine sandpaper. Figure 4a shows a photograph of the board. The accuracy of the two fibers are evaluated

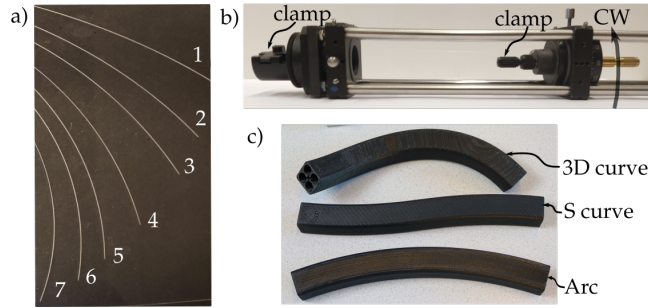


Figure 4: a) Slots of fixed curvature on an acrylic board used for determining curvature accuracy of the two multi-core fibers. Each slot is numbered and has a unique curvature in the range from  $1.33 \text{ m}^{-1}$  to  $5.71 \text{ m}^{-1}$ . b) A cage mechanism where a fiber can be clamped such that one end is fixed and the other end can be rotated. This setup is utilized for the twist experiments, where the fiber is rotated in clockwise (CW) and counter-clockwise (CCW) directions in steps of  $10^\circ$ . The distance between the two clamps is 175 mm. c) The three moulds used for the pose experiments. The arc has a constant curvature of  $3.33 \text{ m}^{-1}$ , the S curve has a linearly changing curvature starting from  $2.5 \text{ m}^{-1}$  to  $-2.5 \text{ m}^{-1}$  and the 3D curve is a helix with radius of  $0.1 \text{ m}$  and pitch of  $2.05 \times 10^{-1} \text{ m}$ .

by placing them in the slots and getting the difference between the measured curvature and the curvature of the slot. Figure 5a plots each slot's curvature as the ground truth and the corresponding calculated curvature using (7), where  $r$  is the center to core distance of the fiber and  $S$  is determined through calibration for each FBG set. The calibration procedure consists of collecting measurements

Table 1: Specifications of the straight and helical multi-core fibers

Core	Sensorized Length	FBG Length	Twist rate	Center to Core
Helical	175 mm	11 mm	50 turns/m	$35 \mu\text{m}$
Straight	115.5 mm	10 mm	N/A	$35 \mu\text{m}$
Core	Cladding diameter	Coating diameter	Core angles	Coating type
Helical	$125 \mu\text{m}$	$200 \mu\text{m}$	$120^\circ$	Acrylate
Straight	$125 \mu\text{m}$	$250 \mu\text{m}$	$120^\circ$	Acrylate

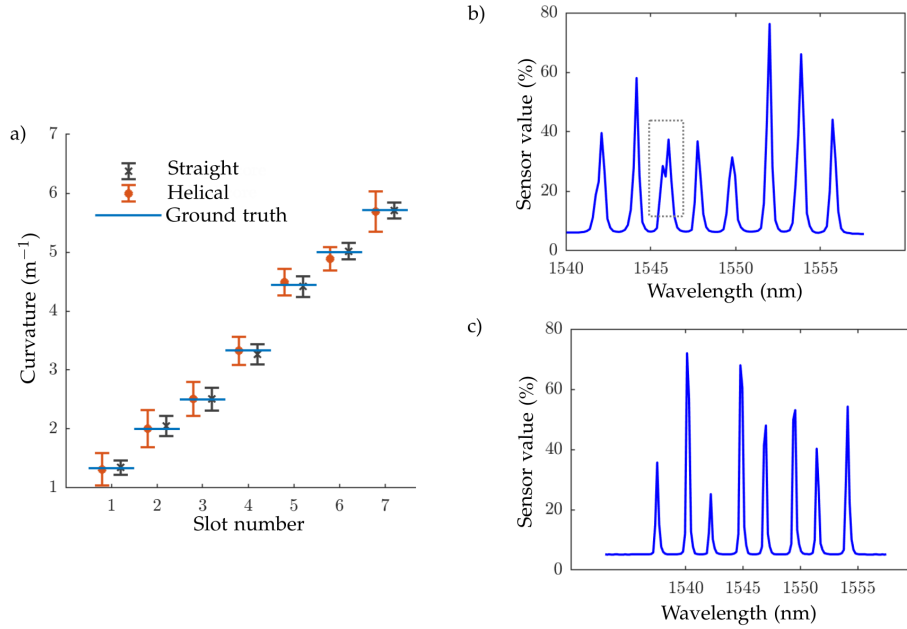


Figure 5: a) The mean and standard deviation of the curvature measurements along with the ground truth. The slot number is a unique number given to each slot with fixed curvature and the slot's curvature is the ground truth value. b) A spectra from fiber Bragg grating sensors on the helical core fiber with double peaks, which are highlighted with a gray dashed box. c) A spectra from fiber Bragg grating sensors on the straight core fiber.

from the fiber and solving for the value of  $S$  that leads to the minimum difference between the measurements and the ground truth. The curvature error measure  $\kappa_e \in \mathbb{R}_{\geq 0}$  utilized is the absolute difference between the ground truth  $\kappa_{gt} \in \mathbb{R}_{\geq 0}$  and the measured curvature  $\kappa_m \in \mathbb{R}_{\geq 0}$  :

$$\kappa_e = |\kappa_{gt} - \kappa_m|, \quad (14)$$

The error  $\kappa_e$  is calculated for each sensor set and the mean error of the sensor sets over all the slots is  $0.22 \text{ m}^{-1}$  and  $0.13 \text{ m}^{-1}$  for helical and straight core fiber, respectively. The standard deviation of the error is  $0.11 \text{ m}^{-1}$  and  $0.07 \text{ m}^{-1}$  for helical and straight core fiber, respectively. The results show that the straight core fiber is more accurate in measuring the curvature however not significantly more. One source of inaccuracy in the helical fiber could be due to multiple

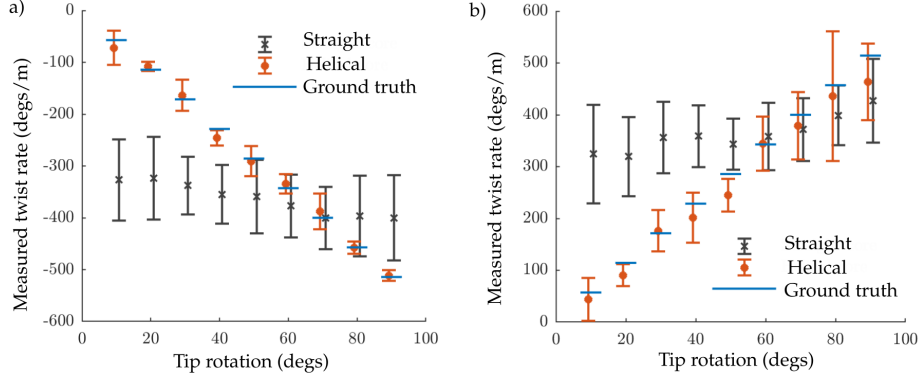


Figure 6: The mean and standard deviation of the twist measurements in clock-wise (a) and counter-clockwise direction (b).

peaks reflected from the sensors when the slot curvature is greater than  $4 \text{ m}^{-1}$ . For this study the mean of the multi-peaks is considered to be the shifted Bragg  
 90 wavelength. Figure 5b illustrates a spectra, where one of the sensors has double peaks. The phenomenon of multiple peaks may be reduced by using apodized FBG sensors.

### 3.2. Twist

The accuracy of measuring twist using the two fibers is determined by clamping one end of the fiber and applying a rotation at the other end, which is the tip of the fiber. This experiment is conducted using an in-house assembled cage mechanism, as shown in Figure 4b. The rotating end of the mechanism consists of a dial with angular graduations of five degrees. During the experiment, the fiber is clamped on both ends and the dial is rotated in steps of  $10^\circ$  from  $10^\circ$  to  $90^\circ$  in clockwise (CW) and counter-clockwise (CCW) directions, as shown in Figure 4b. The error in twist measurement  $\phi_e \in \mathbb{R}$  is determined by the absolute difference between the applied twist  $\phi_{app} \in \mathbb{R}$  and the measured twist  $\phi_m \in \mathbb{R}$  as per the following equation:

$$\phi_e = |\phi_{app} - \phi_m|, \quad (15)$$

The measured twist  $\phi_m$  is calculated using (8), where  $\Delta z$  is the distance between  
95 the FBG sensor sets,  $r$  is the center to core distance.  $G$  is determined by  
calibration where a set of experiment data is used to find the value of  $G$  for  
which the twist error is minimized. Figure 6 shows the plot of the ground truth,  
which is the applied twist, and the measured twist for both the straight and  
helical core fiber. The applied twist along the fiber is related to the tip rotation  
100 as:  $\phi_{app} = \theta_t/L$  where,  $\theta_t \in \mathbb{R}$  is the tip rotation and  $L$  is 175 mm since that is  
the fiber length over which the twist is applied. The mean twist error is 26.57  
degrees/m and 146.50 degrees/m for helical and straight core fibers, respectively.  
The standard deviation in twist error is 29.96 degrees/m and 59.74 degrees/m  
for helical and straight core fibers, respectively.

105 The results show that the helical core fiber can measure the twist with more  
accuracy than the straight core fiber. This is because with the straight core the  
FBG sensing of shear strain is very low whereas in helical core since the FBGs are  
on a helix the twist translates into elongation thus the FBG sensors register the  
shear strain more accurately. Another observation is that the helical core fiber  
110 does not have a symmetric response for clockwise and counter-clockwise twist.  
This could be due to the non-symmetric response of the sensors to elongation  
and compression.

### 3.3. Pose

In this experiment, each of the two fibers is placed in a catheter which is then  
115 placed in three moulds with the following center-line curve: arc, S curve and 3D  
curve, as shown in Figure 4c. The arc is a planar curve with a constant curvature  
of  $3.33 \text{ m}^{-1}$ , the S curve is also a planar curve with curvature changing from  $2.5$   
 $\text{m}^{-1}$  to  $-2.5 \text{ m}^{-1}$ , lastly the 3D curve is a segment of a helix with radius of  $0.1$   
m and pitch of  $2.05 \times 10^{-1} \text{ m}$ . Thus, the tip pose of the three curves are known  
120 and utilized as ground truths. The tip pose of the fiber is acquired using (13),  
where  $\psi[n]$  is found by placing the fiber in a fixed curvature slot and calculating  
the difference between the measured frame and the actual frame. Moreover, the  
fiber tip position  $\mathbf{r} \in \mathbb{R}^3$  is  $\gamma(L)$ , where  $L$  is the length from the first sensor

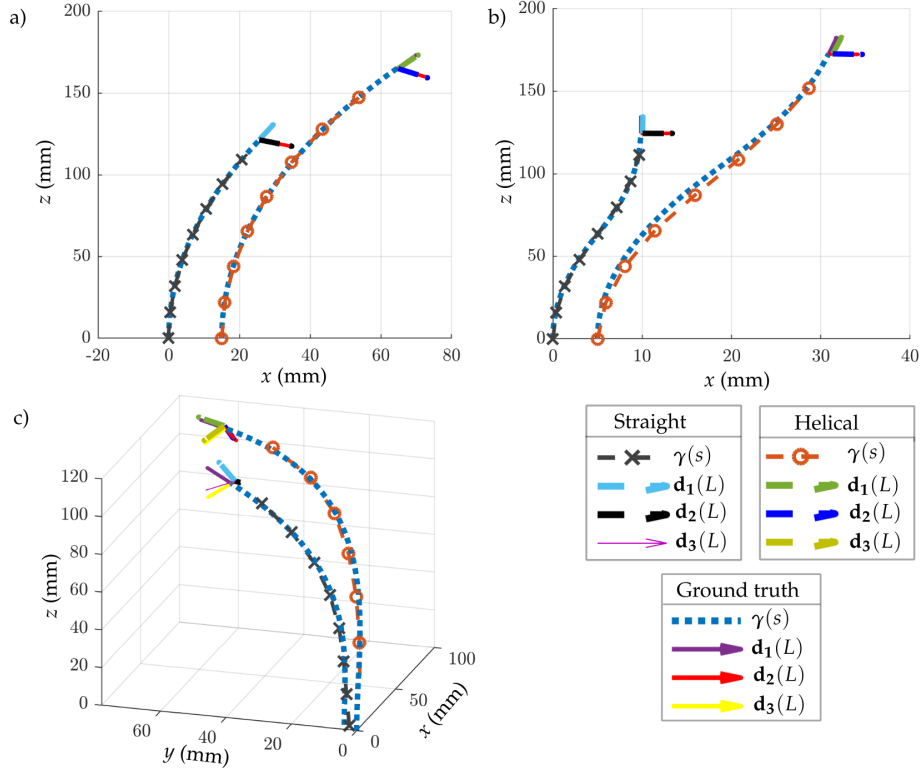


Figure 7: The pose measurement based on the fiber Bragg grating sensors and the ground truth for the three moulds. The helical core measurements in the plots are shifted about the  $x$  axis for visual clarity. The curves for the straight core fiber is shorter than the helical core fiber because the sensorized length of the straight and helical core fiber are 115.5 mm and 175 mm, respectively. The tip pose and the center-line of the straight and helical core fiber for the arc, S curve and 3D curve are shown in (a), (b) and (c), respectively.

set to the last. The orientation of the fiber tip is given by the material frames  
125  $\mathbf{d}_1$ ,  $\mathbf{d}_2$ ,  $\mathbf{d}_3$ , since they are orthonormal they form an orientation matrix and the  
orientation at the tip is given by the matrix  $[\mathbf{d}_1(L) \ \mathbf{d}_2(L) \ \mathbf{d}_3(L)]$ . For error  
calculations we use axis-angle representation of orientation that is derived from  
the tip orientation matrix [19]. The axis which is the tip orientation vector  
is given as  $\mathbf{v} \in \mathbb{R}^3$  and the angle which is the angle of rotation about the  
130 orientation vector is given as  $\omega \in \mathbb{R}$ . The pose error measures are calculated as  
follows [18]:

$$r_e = \|\mathbf{r} - \mathbf{r}_{gt}\| \quad (16)$$

$$v_e = \cos^{-1} \left( \frac{\mathbf{v}_{gt} \cdot \mathbf{v}}{\|\mathbf{v}_{gt}\| \|\mathbf{v}\|} \right) \quad (17)$$

$$\omega_e = \|\omega - \omega_{gt}\| \quad (18)$$

where,  $\mathbf{r}_{gt} \in \mathbb{R}^3$  is the ground truth of the tip position,  $\mathbf{v}_{gt} \in \mathbb{R}^3$  is the true orientation vector and  $\omega_{gt} \in \mathbb{R}$  is the angle of rotation about the true orientation vector. The catheter with the fiber is inserted in each mould five times. Table 2 gives the mean pose errors and the standard deviation over all the trials. Figure 7 shows the reconstructions of the three curves and the tip pose for one of the trials. The results show that both the fibers have similar error measures, however the helical core fiber gives a slightly lower error in orientation for the space curve pose.

#### 4. Conclusions

In this study, multi-core fibers with FBG sensors are utilized to acquire curvature, twist and pose measurements. Moreover, the accuracy of the measurements from the FBG sensors in a helical core fiber is compared to that of the sensors in a straight core fiber. The mean error in curvature for helical and straight core fiber are  $0.22 \text{ m}^{-1}$  and  $0.13 \text{ m}^{-1}$ , respectively, whereas in twist measurement the mean error measures are  $26.57 \text{ degrees/m}$  and  $146.50 \text{ degrees/m}$ , respectively. Lastly, the mean error in position for the helical and

Table 2: The mean and standard deviation in brackets over multiple trials of the position, axis and angle error according to (16)- (18), respectively.

	Helical	Straight
$r_e$ (mm)	0.49 (0.24)	0.27 (0.14)
$v_e$ (degs)	0.12 (0.16)	0.26 (0.14)
$\omega_e$ (degs)	1.10 (0.71)	1.18 (1.06)

straight core fiber are 0.49 mm and 0.27 mm, respectively; in axis orientation is 0.12 degrees and 0.26 degrees; and in angle orientation is 1.10 degrees and 1.18 degrees, respectively. The accuracy for the pose measurement is similar for both  
150 fibers. However, for applications with twist, FBG sensors on helical core fiber will produce more accurate results than FBG sensors on straight core fiber.

### Acknowledgements

The authors would like to thank Francis Kalloor Joseph and Frans Segerink  
155 from University of Twente for their assistance in building the twist experiment setup. In addition, the authors really appreciate the assistance provided by Fujikura in understanding the spectra from the helical core fibers and by FBGS International NV with the strain to wavelength equation.

### Author contributions

**Fouzia Khan:** Conceptualization, methodology, software, validation, formal analysis, investigation, resources, data curation, writing–original draft preparation, writing–review and editing. **David Barrera:** Formal analysis, investigation, resources, writing–review and editing. **Salvador Sales:** Writing–review and editing, supervision, project administration, funding acquisition. **Sarthak  
165 Misra:** Conceptualization, writing–review and editing, supervision, project administration, funding acquisition.

### Appendix A.

The derivation of (5)-(8) is given in this appendix. The curvature and twist are evaluated from the Bragg wavelength measurements of the FBG sensors. First, the strain on the fiber is calculated from the wavelength measurements and then the curvature and twist is evaluated from the strain using material mechanics [15]. The relation between the strain and the wavelength is given in (4) as:

$$\ln \frac{\lambda_B}{\lambda_{B0}} = S(\epsilon - \epsilon_0) + \Sigma(T - T_0), \quad (\text{A.1})$$



The left hand side of (A.1) is a direct measurement from the sensors. Let  $i \in \{1, 2, 3, 4\}$  represent the FBG sensor number,

$$\ln \frac{\lambda_{Bi}}{\lambda_{B0i}} = m_i, \quad \text{and} \quad (\text{A.2})$$

$$S(\epsilon_i - \epsilon_{0i}) = S(\epsilon_{i\kappa} + \epsilon_\tau) = m_{i\Delta\epsilon}, \quad (\text{A.3})$$

where  $m_i \in \mathbb{R}$ , (A.3) is based on  $\epsilon_{0i} = 0$  which is true if  $\lambda_{B0i}$  is measured when fiber is stress-free.  $\epsilon_{i\kappa} \in \mathbb{R}$  is strain due to curvature and  $\epsilon_\tau$  is axial twist strain which is the same in sensors 1, 2 and 3. All four FBG sensors will experience the same temperature change because they are close in proximity, thus the value of the term  $\Sigma(T - T_0)$  is the same in all sensors. Moreover, sensor 4 theoretically will be strain free because it is in the center of the fiber, thus:

$$\Sigma(T_i - T_{0i}) = m_4. \quad (\text{A.4})$$

$$\epsilon_{i\kappa} = -\kappa r \cos\left(\theta_1 + \frac{2\pi}{3}(i-1)\right), \quad (\text{A.5})$$

where  $\epsilon_{i\kappa} \in \mathbb{R}$  is the strain is sensor  $i \in \{1, 2, 3\}$ ;  $\epsilon_{4\kappa} = 0$ . (A.5) is based on material mechanics, for further details see Khan *et. al* [1]. The following holds for sensors  $i \in \{1, 2, 3\}$  using (A.2)-(A.3):

$$m_i = m_{i\Delta\epsilon} + m_4 \quad (\text{A.6})$$

Substituting (A.3), (A.5) into (A.6) and applying trigonometric angle sum identities the following holds:

$$m_1 - m_4 = m_{1\Delta\epsilon} = S(-\kappa r \cos(\theta_1) + \epsilon_\tau) \quad (\text{A.7})$$

$$m_2 - m_4 = m_{2\Delta\epsilon} = S\left(\frac{1}{2}\kappa r \cos(\theta_1) + \frac{\sqrt{3}}{2}\sin(\theta_1) + \epsilon_\tau\right) \quad (\text{A.8})$$

$$m_3 - m_4 = m_{3\Delta\epsilon} = S\left(\frac{1}{2}\kappa r \cos(\theta_1) - \frac{\sqrt{3}}{2}\sin(\theta_1) + \epsilon_\tau\right) \quad (\text{A.9})$$

Summing (A.7)- (A.9) leads to the trigonometry terms to add to zero and the following is achieved:

$$\frac{1}{3S} \sum_{i=1}^3 m_{i\Delta\epsilon} = \epsilon_\tau \quad (\text{A.10})$$

Thus, the strain due to twist can be calculated using (A.10) and the twist can be calculated by rearranging (2) into:

$$\Delta\phi = \epsilon_\tau \frac{\Delta z}{Gr}, \quad (\text{A.11})$$

which is the twist equation (8). The curvature value can be solved by rearranging (A.7)- (A.9) as

$$\zeta = \mathbf{C}\mathbf{v}, \quad (\text{A.12})$$

$$\text{where, } \zeta = \begin{bmatrix} \zeta_1 \\ \zeta_2 \\ \zeta_3 \end{bmatrix} = \begin{bmatrix} m_1 - m_4 - S\epsilon_\tau \\ m_2 - m_4 - S\epsilon_\tau \\ m_3 - m_4 - S\epsilon_\tau \end{bmatrix} \quad \mathbf{C} = \begin{bmatrix} -Sr & 0 \\ \frac{1}{2}Sr & \frac{\sqrt{3}}{2}Sr \\ \frac{1}{2}Sr & -\frac{\sqrt{3}}{2}Sr \end{bmatrix}$$

$$\mathbf{v} = \begin{bmatrix} v_1 \\ v_2 \end{bmatrix} = \begin{bmatrix} \kappa \cos(\theta_1) \\ \kappa \sin(\theta_1) \end{bmatrix}$$

Then  $v = \mathbf{C}^\dagger \zeta$ , where  $\mathbf{C}^\dagger$  is the Moore-Penrose pseudo-inverse of  $\mathbf{C}$  and

$$\kappa = \|\mathbf{v}\| = \sqrt{v_1^2 + v_2^2} \quad (\text{A.13})$$

gives the curvature equation (7).

## References

- 170 [1] F. Khan, A. Denasi, D. Barrera, J. Madrigal, S. Sales, S. Misra, Multi-core optical fibers with Bragg gratings as shape sensor for flexible medical instruments, *IEEE Sensors Journal* 19 (14) (2019) 5878–5884.
- [2] P. S. Westbrook, T. Kremp, K. S. Feder, W. Ko, E. M. Monberg, H. Wu, D. A. Simoff, T. F. Taunay, R. M. Ortiz, Continuous multicore optical fiber grating arrays for distributed sensing applications, *Journal of Lightwave Technology* 35 (6) (2017) 1248–1252.
- 175 [3] A. Wolf, A. Dostovalov, K. Bronnikov, S. Babin, Arrays of fiber Bragg gratings selectively inscribed in different cores of 7-core spun optical fiber by IR femtosecond laser pulses, *Opt. Express* 27 (10) (2019) 13978–13990.

- 180 [4] C. G. Askins, G. A. Miller, E. J. Friebele, Bend and twist sensing in a multi-core optical fiber, in: LEOS 2008 - 21st Annual Meeting of the IEEE Lasers and Electro-Optics Society, 2008, pp. 109–110.
- [5] J. P. Moore, M. D. Rogge, Shape sensing using multi-core fiber optic cable and parametric curve solutions, *Opt. Express* 20 (3) (2012) 2967–2973.
- 185 [6] S. Jäckle, T. Eixmann, H. Schulz-Hildebrandt, G. Hüttmann, T. Pätz, Fiber optical shape sensing of flexible instruments for endovascular navigation, *International Journal of Computer Assisted Radiology and Surgery* 14 (2019) 2137–2145.
- [7] R. Xu, A. Yurkewich, R. V. Patel, Curvature, torsion, and force sensing  
190 in continuum robots using helically wrapped FBG sensors, *IEEE Robotics and Automation Letters* 1 (2) (2016) 1052–1059.
- [8] R. J. Roesthuis, M. Kemp, J. J. van den Dobbelsteen, S. Misra, Three-dimensional needle shape reconstruction using an array of fiber Bragg grating sensors, *IEEE/ASME Transactions on Mechatronics* 19 (4) (2014)  
195 1115–1126.
- [9] R. G. Duncan, M. T. Raum, Characterization of a fiber-optic shape and position sensor, in: *Smart Structures and Materials 2006: Smart Sensor Monitoring Systems and Applications*, 2006, pp. 26–36.
- [10] Y. Wang, C. Xu, V. Izraelian, Bragg gratings in spun fibers, *IEEE Photonics Technology Letters* 17 (6) (2005) 1220–1222.  
200
- [11] H. Zhang, Z. Wu, P. P. Shum, X. Shao, R. Wang, X. Q. Dinh, S. Fu, W. Tong, M. Tang, Directional torsion and temperature discrimination based on a multicore fiber with a helical structure, *Opt. Express* 26 (1) (2018) 544–551.
- 205 [12] I. Floris, J. Madrigal, S. Sales, P. A. Calderòn, J. M. Adam, Twisting compensation of optical multicore fiber shape sensors for flexible medical

- instruments, in: *Optical Fibers and Sensors for Medical Diagnostics and Treatment Applications XX*, 2020, pp. 128–132.
- [13] V. Budinski, D. Donlagic, Fiber-optic sensors for measurements of torsion, twist and rotation: A review, *Sensors (Basel)* 17 (3) (2017) 443–472.
- [14] B. Audoly, Y. Pomeau, *Elasticity and geometry : From hair curls to the non-linear response of shells*, Oxford University Press, New York, 2010.
- [15] R. C. Hibbeler, *Mechanics of Materials 8th ed.*, Pearson Prentice Hall, Upper Saddle River, New Jersey, 2011.
- [16] R. J. Roesthuis, S. Janssen, S. Misra, On using an array of fiber Bragg grating sensors for closed-loop control of flexible minimally invasive surgical instruments, in: *2013 IEEE/RSJ International Conference on Intelligent Robots and Systems*, 2013, pp. 2545–2551.
- [17] J. V. Roosbroeck, C. Chojetzki, J. Vlekken, E. Voet, M. Voet, A new methodology for fiber optic strain gage measurements and its characterization, in: *SENSOR+TEST Conferences*, vol. OPTO 2 - Optical Fiber Sensors, 2009, pp. 59–64.
- [18] F. Khan, A. Donder, S. Galvan, F. Rodriguez y Baena, S. Misra, Pose measurement of flexible medical instruments using fiber Bragg gratings in multi-core fiber, *IEEE Sensors Journal* In Press DOI:10.1109/JSEN.2020.2993452 (2020).
- [19] J. J. Craig, *Introduction to Robotics: Mechanics and Control*, third ed., Pearson Prentice Hall, Upper Saddle River, New Jersey, 2005.